Journal of Taibah University for Science

ISSN: (Print) (Online) Journal homepage: www.tandfonline.com/journals/tusc20

Promising reddish-orange light as Eu^{3+} incorporated in zinc-borosilicate glass derived from the waste glass bottle

Wei Mun Cheong, Mohd Hafiz Mohd Zaid, Khamirul Amin Matori, Yap Wing Fen, Tan Sin Tee, Zhi Wei Loh & Mohd Zul Hilmi Mayzan

To cite this article: Wei Mun Cheong, Mohd Hafiz Mohd Zaid, Khamirul Amin Matori, Yap Wing Fen, Tan Sin Tee, Zhi Wei Loh & Mohd Zul Hilmi Mayzan (2023) Promising reddish-orange light as Eu^{3+} incorporated in zinc-borosilicate glass derived from the waste glass bottle, Journal of Taibah University for Science, 17:1, 2260080, DOI: 10.1080/16583655.2023.2260080

To link to this article: https://doi.org/10.1080/16583655.2023.2260080

Published online: 19 Sep 2023.

JOURNAL OF TAIBAH UNIVERSITY FOR SCIENCE
2023, VOL. 17, NO. 1, 2260080
https://doi.org/10.1080/16583655.2023.2260080

JTUSCI

Journal of Taibah University for Science

Taylor & Francis
Taylor & Francis Group

OPEN ACCESS Check for updates

Promising reddish-orange light as Eu^{3+} incorporated in zinc-borosilicate glass derived from the waste glass bottle

Wei Mun Cheong[a], Mohd Hafiz Mohd Zaid [a,b], Khamirul Amin Matori[a,b], Yap Wing Fen[a], Tan Sin Tee[a], Zhi Wei Loh[a] and Mohd Zul Hilmi Mayzan[c]

[a]Department of Physics, Faculty of Science, Universiti Putra Malaysia, UPM, Serdang, Selangor, Malaysia; [b]Nanomaterials Synthesis and Characterization Laboratory, Institute of Nanoscience and Nanotechnology, Universiti Putra Malaysia, UPM, Serdang, Selangor, Malaysia; [c]Ceramic and Amorphous Group (CerAm), Faculty of Applied Sciences and Technology, Pagoh Higher Education Hub, Universiti Tun Hussein Onn Malaysia, Panchor, Johor, Malaysia

ABSTRACT

Eu^{3+} incorporated zinc-borosilicate glass was synthesized using melt-quenching method. XRD and FTIR verified the amorphous nature of the samples. The absorption spectra indicate the Eu^{3+} ions in the UV-visible region at ~394 nm. The direct and indirect band gap decrease from 5.152 eV to 5.082 eV and 4.133 eV to 3.837 eV, respectively. Meanwhile, the refractive index decrease from 2.145 to 2.202, while the Urbach energy ranges from 0.682 eV to 0.733 eV. All the samples have a good transmission percentage at 70–75%. Under the excitation of 400 nm, the intensity of the PL spectra increased when the Eu^{3+} dopant increased. The optimum content for Eu^{3+} incorporated $ZnO–B_2O_3–GB$ glass is 3 wt.% among the other Eu^{3+} content (0, 1, and 2 wt.%) in this work. The reddish-orange emission at 612 nm ($^5D_0 \rightarrow {}^7F_2$) indicates the most intense emission and the CIE chromaticity coordinates imply in the reddish-orange region.

ARTICLE HISTORY
Received 20 April 2022
Revised 22 March 2023
Accepted 5 September 2023

KEYWORDS
Glass waste; Eu^{3+} dopant; Energy transfer; Luminescence; CIE chromaticity

1. Introduction

Across the years, luminescent materials have been effectively employed in optoelectronics, photonics, and solid-state lasers. Due to their energy consumption, brightness, long lifetime, and being environmentally friendly, researchers worldwide focus on optoelectronic applications, such as light-emitting diode (LED), solid-state lighting, and fluorescent display devices [1,2]. In addition, luminescent materials have a wide application which also can be applied in biosensing and bioimaging, phototherapy, data storage, security technologies, optical temperature sensors, and fluorescent thermometers [3–7]. The luminous material's capabilities are deeply controlled by the active centres, the host material, and their interaction [8]. Meanwhile, glass is critical for optical material applications due to its excellent transparency in the visible region. The typical material fabricating glass bottles is soda-lime-silica, consisting of 70.5% SiO_2, 12.5% Na_2O, 11.3% CaO, and 2.8% Al_2O_3 [9,10]. Unfortunately, waste glass bottles are one of the toughest to recycle [11]. Therefore, this work uses the waste glass bottles as the SiO_2 source to fabricate zinc-borosilicate glass ($ZnO–B_2O_3–GB$). Glasses made of zinc-borosilicate are noteworthy for their thermal shock resistance, strong elastic modulus, chemical resistance, and piezoelectric characteristics [12]. Nevertheless, zinc-borosilicate glass's low energy absorption rates have restricted its applicability. Introducing rare-earth ions into the host glass is one method for resolving this issue.

The glass matrix incorporated with rare-earth ions exhibits outstanding optical properties, including excellent resistance to laser amplification and high quantum efficiency [13]. Eu^{3+} ions stand out among the rare-earth ions as an activator with bright orange and red emissions due to the $4f \rightarrow 4f$ electronic transition across the $^5D_0 \rightarrow {}^7F_J$ transition, where $\Delta J = 0$ to 6. In addition, Eu^{3+} ions are also utilized in various technological uses due to their reputed electric dipole transition $^5D_0 \rightarrow {}^7F_2$ (~611 nm), resulting in a consistent perfect red light-emitting centre for the display system [14,15]. From the literature, the chemical environment affects the intensity of this hypersensitive electric dipole transition, whereas the magnetic dipole transition $^5D_0 \rightarrow {}^7F_1$ (~593 nm) is unaffected by the local ligand field [16].

To the best of our knowledge, the zinc-borosilicate glass system incorporated rare earth has been extensively explored for its photoluminescence capabilities. This paper describes the synthesis of Eu^{3+} incorporated zinc-borosilicate glass derived from waste glass bottles via the melt-quenching method. In addition, the effect of the Eu^{3+} dopant on the structural, optical, and luminescence properties was explored. The novel material developed in this work is prospective to be utilized as

CONTACT Mohd Hafiz Mohd Zaid mhmzaid@upm.edu.my Department of Physics, Faculty of Science, Universiti Putra Malaysia, UPM, 43400 Serdang, Selangor, Malaysia Nanomaterials Synthesis and Characterization Laboratory, Institute of Nanoscience and Nanotechnology, Universiti Putra Malaysia, 43400 Serdang, Selangor, Malaysia

a reddish-orange phosphor material in optoelectronic devices such as LEDs.

2. Methodology

2.1. Samples preparation

The melt-quenching method was utilized to synthesize the europium incorporated zinc-borosilicate glass, with the empirical formula, $[Eu_2O_3]_x[(ZnO)_{0.5}(B_2O_3)_{0.1}(GB)_{0.4}]_{1-x}$, where $x = 0, 0.01, 0.02, 0.03$ in weight percent as presented in Table 1. The raw materials selected were zinc oxide (Sigma-Aldrich, 99.9%), boron oxide (Acros Organics, 98%), waste transparent glass bottle as the source of SiO_2, and europium (III) $oxide_3$ (Alfa Aesar, 99.99%) powders. The cleaned glass bottles (GB) were first crushed using a plunger, ground with a mortar and pestle, and then sieved into 45 µm to obtain a fine powder. After that, the obtained glass bottle powder, zinc oxide, boron oxide, and europium (III) oxide powder were mixed and milled to get homogeneous powders. Next, the alumina crucible with the mixture was melted at 1300 °C at 10 °C/min and held for 2 h at a high-temperature electrical furnace. Meanwhile, to eliminate bubbles from the glass melt, the crucible was swirled twice during the melting process before the quenching process. Next, the glass melts were quenched in another furnace using a prepared stainless-steel mold and then annealed for an hour at 400 °C to eliminate any tiny bubbles in the glass and prevent it from thermal shock.

2.2. Characterization

In the present work, the glassy phases of the samples were determined by X-ray diffraction (XRD) through PANalytical (Philips) X' Pert Pro PW3050/6 in powders form via Ni-filtered Cu-Kα radiation. The 2θ scans were performed which scanned at 2θ, which is 20° to 80°. Besides, the molecular vibrations of the samples were investigated via Perkin Elmer Spectrum Two Fourier transform spectrometer (FTIR) with a wavenumber of 4000–400 cm^{-1}. Meanwhile, the optical absorbance and reflectance of the glass sample were determined using UV-Vis spectroscopy with a transmission range of 220–1000 nm. Likewise, the photoluminescence excitation (PLE) the photoluminescence emission was determined using a photoluminescence spectrometer, model Perkin Elmer LS 55. Finally, the CIE chromaticity coordination of the sample was calculated using obtained PL results, which also included the glass samples' dominant wavelength, CCT, and colour purity.

Table 1. The glass sample's composition.

Glass sample code	Glass composition
ZBS	$(ZnO)_{0.5}(B_2O_3)_{0.1}(GB)_{0.4}$
1Eu	$[Eu_2O_3]_{0.01}[(ZnO)_{0.5}(B_2O_3)_{0.1}(GB)_{0.4}]_{0.99}$
2Eu	$[Eu_2O_3]_{0.02}[(ZnO)_{0.5}(B_2O_3)_{0.1}(GB)_{0.4}]_{0.98}$
3Eu	$[Eu_2O_3]_{0.03}[(ZnO)_{0.5}(B_2O_3)_{0.1}(GB)_{0.4}]_{0.97}$

3. Result and discussion

3.1. X-ray diffraction (XRD) analysis

Figure 1 indicates the X-ray diffraction of $ZnO–B_2O_3–GB$ incorporated with different Eu^{3+} content. From the figure, all the glass samples exhibit similar x-ray diffraction with a massive hump from 20° to 40°. Additionally, no continuous sharp peaks appear, revealing the glass system's dominance of glassy structural arrangement, and no crystalline is formed. Commonly, the absence of well-defined planes and a consistent structure arrangement on or surrounding the glass samples defines amorphous glass structures [17]. Therefore, the glass samples showed a completely amorphous phase in nature.

3.2. Fourier transform infrared spectroscopy (FTIR) analysis

Figure 2 depicts the FTIR spectra of $ZnO–B_2O_3–GB$ incorporated with different Eu^{3+} content, and the vibrational modes for FTIR spectra are summarized in Table 2. FTIR spectra generally reveal information about the functional groups that appear in a system, the molecular geometry, and intra- or intermolecular interactions

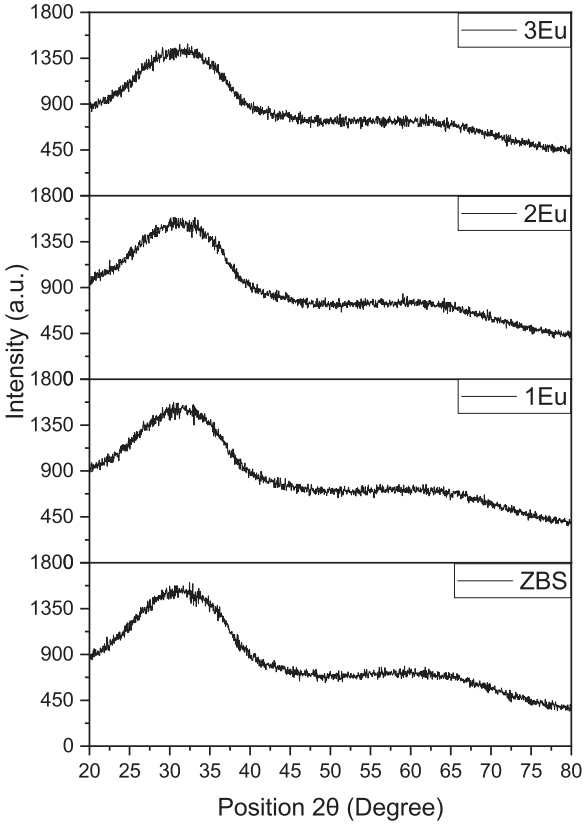

Figure 1. X-ray diffraction of $ZnO–B_2O_3–GB$ incorporated with different Eu^{3+} content.

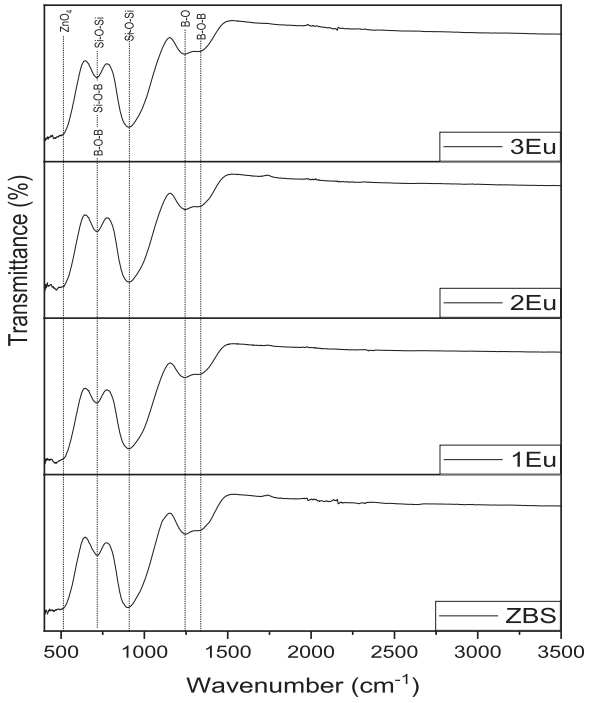

Figure 2. FTIR spectra of ZnO–B_2O_3–GB incorporated with different Eu^{3+} content.

[18]. As seen in Figure 2, the FTIR spectra of all the glass samples demonstrate a repeating pattern with five bands at ~512 cm^{-1}, ~715 cm^{-1}, ~908 cm^{-1}, ~1248 cm^{-1}, and ~1337 cm^{-1}. The band at ~512 cm^{-1} originated from the ZnO_4 group of symmetric stretching vibration modes [19]. Likewise, the bands of 715 cm^{-1} and ~908 cm^{-1} corresponded to the Si–O–Si symmetric stretching vibration [20] and Si–O–Si asymmetric stretching vibrations of SiO_4 tetrahedron [21]. The appearance of these absorption bands illustrates the presence of silica in the glass bottle powder. On the other hand, the bands ~715 cm^{-1} and ~904 cm^{-1} were induced by Si–O–Si symmetric stretching vibration [20] and Si–O–Si asymmetric stretching vibrations of SiO_4 tetrahedron [21], respectively. These infrared absorption bands are indicated by the existence of silica in SLS glass powder. The three SiO_4 and ZnO_4 bands show no zinc silicate glass-ceramics formed, consistent with the XRD pattern, which indicated that all samples are amorphous. Furthermore, the asymmetric stretching vibrations of BO_4 units in the borate network can be identified at the wavenumber between 900 and 1000 cm^{-1}, which superimposes the silicate network's vibrations [22]. Thus, the bands ~715 cm^{-1}, ~1244 cm^{-1}, and ~1337 cm^{-1} induced B–O–B bending vibration of BO_3 triangles and B–O rings of BO_3 and BO_4 units [22], and asymmetric stretching vibration of B–O–B in BO_3 units, respectively [23]. Moreover, the ~715 cm^{-1} also ascribed Si–O–B linkages. Meanwhile, the FTIR could not discover the band of Eu^{3+} in the glass samples designated 1Eu, 2Eu, and 3Eu. It is believed that this situation occurs because of a slight concentration of Eu^{3+} incorporated into the glass sample and entirely dissolved in the glass samples. Khaidir et al. also reported a similar observation [24]. According to the glass theory, Eu^{3+} serves as a network modifier and can be attracted by the borate network. The non-bridging oxygens (NBOs) are taken up by BO_3 groups, resulting in the formation of BO_4 groups, which are negatively charged and cannot connect directly to one another. Thus, at 1244 cm^{-1}, BO_4 groups can join BO_3 groups and create boron-oxygen (B–O) rings [22].

3.3. Optical absorption analysis

The UV-Vis absorbance spectra of ZnO–B_2O_3–GB incorporated with different Eu^{3+} content from 250 nm to 1000 nm are shown in Figure 3 The transition of Eu^{3+} illustrated in the UV-visible region at about 394 nm indicates the transition of $^7F_0 \rightarrow {}^5L_6$, attributed to the 4f–4f transition [25]. This $^7F_0 \rightarrow {}^5L_6$ transition is related to the forbidden transition by ΔS and ΔL selection rules but allowed by the ΔJ selection rule [26]. The mentioned transition is identical in all glass samples containing Eu^{3+} dopant designated 1Eu, 2Eu, and 3Eu. Furthermore, absorbance spectra reveal the samples' amorphous nature due to the absence of well-defined absorption edges, as agreed by XRD analysis. The absorption edges slightly shift to a longer wavelength as the Eu^{3+} dopant increases. This tendency can be attributed to the glass structure's decreased rigidity due to the formation of NBOs in the glass networks [27], which FTIR proves. As the electron bonding of NBOs is less tightly packed than that of bridging oxygens (BOs), the glass networks become weaker. This may be due to the oxygen bonds' strength affecting the absorption edge of the glass system [28].

Table 2. Vibrational mode for FTIR spectra of ZnO–B_2O_3–GB incorporated with different Eu^{3+} content.

Wavenumbers (cm^{-1})	Vibrational mode assignment	References
512	ZnO_4 group symmetric stretching vibration	[19]
715	Si–O–Si symmetric stretching vibration; Si–O–B linkages; B–O–B bending vibration in BO_3	[20]
900–1000	BO_4 asymmetric stretching vibrations	[22]
908	Si–O–Si asymmetric stretching vibrations of SiO_4	[21]
1244	B–O rings of vibration in BO_3 and BO_4	[22]
1337	B–O– B asymmetric stretching vibration in BO_3	[23]

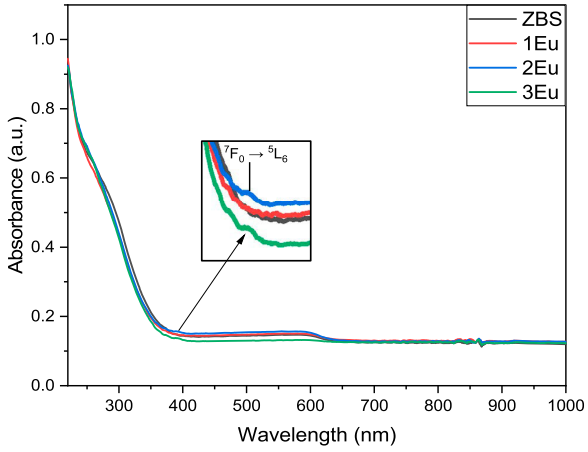

Figure 3. Absorbance spectra of ZnO–B_2O_3–GB incorporated with different Eu^{3+} content.

3.4. Optical band gap analysis

Kubelka-Munk's equation was utilized to evaluate the optical band gap of the samples. The UV-Vis reflectance spectra were transformed to the Kubelka-Munk function using the following equation (1) [29]:

$$F(R) = \frac{K}{S} = \frac{(1-R)^2}{2R} \tag{1}$$

where R = sample's reflectance, K = Absorption coefficient, S = scattering coefficient. The Tauc equation as follows is used to determine the relationship between the band gap energy E_g and the linear absorption coefficient α of a material [30]:

$$(\alpha hv)^{1/n} = B(hv - E_g) \tag{2}$$

where α = absorption coefficient, B = energy-inde pendent constant, h = Plank's constant, v = photon's frequency, and E_g = band gap energy. Now, knowing that F(R) is proportional to α and that equation (3),

$$[F(R)hv]^{1/n} = B(hv - E_g) \tag{3}$$

where $n = \frac{1}{2}$ and $n = 2$ correspond to direct allowed transition and indirect allowed transition. Then, the band gap of the glass samples was estimated by extrapolating the linear region of the Tauc plot to the x-axis, where $[F(R)hv]^{1/n} = 0$. Finally, the Tauc graph for direct and indirect allowed transition band gap is depicted in Figure 4, and the results are summarized in Table 3.

Based on Figure 4, as the Eu^{3+} content increased, the optical band gap for both direct and indirect allowed transition indicates a decreasing trend, from 5.152 eV to 5.082 eV and 4.133 eV to 3.837 eV, respectively. Previous research also reported a similar observation [31]. The increase in Eu^{3+} content will lead to the rise in NBOs, resulting in the glass structure becoming more disordered. Eu^{3+} ions, which behave as a network modifier in the glass system, have destroyed the creation of BOs. It is also reflected in alterations to the glass matrix's arrangement. In addition, incorporating Eu^{3+} ions in the glass network increased the number of free electrons, decreasing the energy band gap [32]. This scenario is due to a rise in matrix disorder, which expands the number of localized states within the E_g [33]. Apart from that, the glass samples exhibit indirect bandgap values between around ~3eV to ~4 eV, comparable to the semiconductor's broad bandgap values (2–4 eV) [26]. As a result, the ZnO–B_2O_3–GB glass incorporated

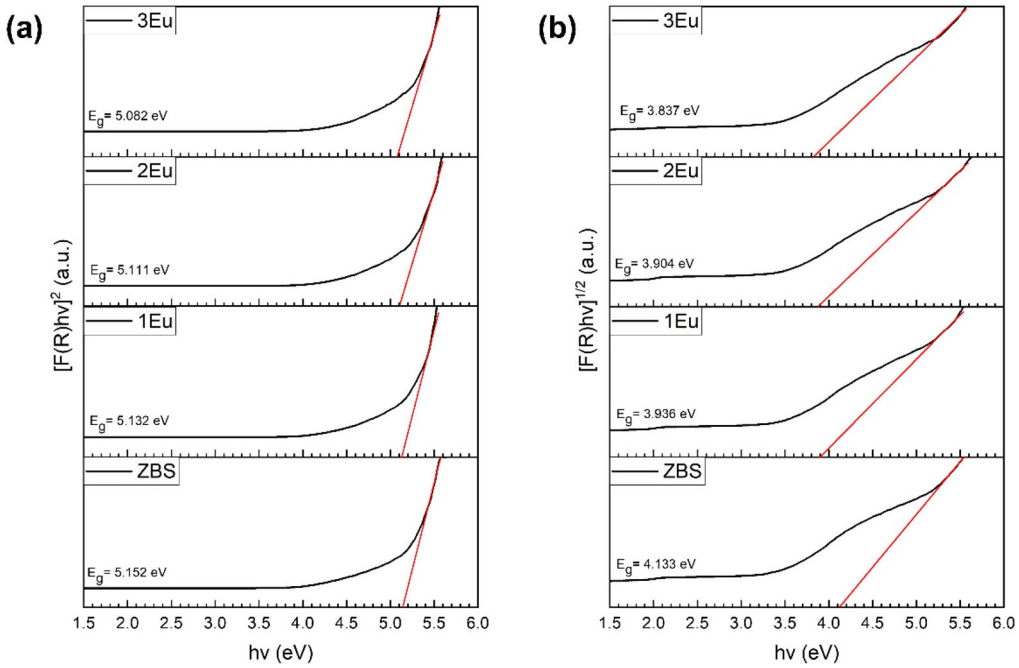

Figure 4. Kubelka-Munk (K-M) plot for (a) direct allowed transition $[F(R)hv]^2$ versus hv, and (b) indirect allowed transition $[F(R)hv]^{1/2}$ versus hv of ZnO–B_2O_3–GB incorporated with different Eu^{3+} content.

Table 3. Optical band gap energy for direct and indirect allowed transition, refractive index, and Urbach energy of the ZnO–B_2O_3–GB incorporated with different Eu^{3+} content.

Glass Sample	Eu^{3+} dopant (wt.%)	Optical band gap energy, E_g (eV)		Refractive index, *n*	Urbach energy, ΔE (eV)
		Direct allowed transition, $n = 1/2$	Indirect allowed transition, $n = 2$		
ZBS	0	5.152	4.133	2.145	0.682
1Eu	1	5.132	3.936	2.182	0.717
2Eu	2	5.111	3.904	2.189	0.726
3Eu	3	5.082	3.837	2.202	0.733

Eu^{3+} potentially reduced the amount of light required for lighting once likened to incandescent lamps and applied in optoelectronic devices such as LEDs.

3.5. Refractive index analysis

The refractive indexes (n) of the glass samples were determined using the Dimitrov and Sakka relation, as shown in the equation (4), to ascertain the uses of the synthesized glass [34].

$$\frac{n^2-1}{n^2+2} = 1 - \sqrt{\frac{E_{opt}}{20}} \tag{4}$$

where n is the samples' refractive index, and E_{opt} denotes the optical band gap energy for the indirect allowed transition of the samples. The plotted refractive index of the ZnO–B_2O_3–GB with different Eu^{3+} content is displayed in Figure 5, and the values are tabulated in Table 3. According to Figure 5 and its refractive index values, an increasing trend in the refractive index can be observed as the progression of Eu^{3+} content, where the refractive index increase from 2.145 to 2.202. This rise in the refractive index could be owing to the combination of samarium oxide with higher polarizability, which produces a vast amount of oxygen ions and alters the coordination numbers [35]. Abu-Khadra et al. [36] also claimed that the increased refractive index behaviour could be attributed to the structural modification due to the incorporation of Eu^{3+}, whereby Eu^{3+} serves as a modifier, raising the NBOs in the glass matrix. As a result, increased non-bridged oxygen will increase ionic bonding, increase the glass system's polarization, and raise the refractive index [37]. In addition, the refractive index of the samples ranges from 2.145–2.202, suggesting the ZnO–B_2O_3–GB incorporated Eu^{3+} potential for photoelectronic applications, as agreed in previous studies [38].

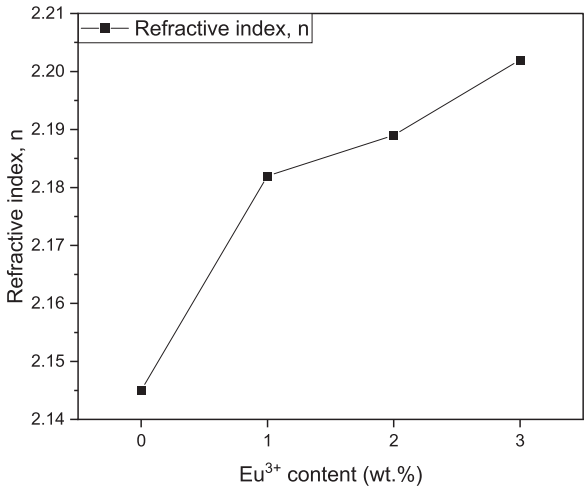

Figure 5. Refractive index of the ZnO–B_2O_3–GB incorporated with different Eu^{3+} content.

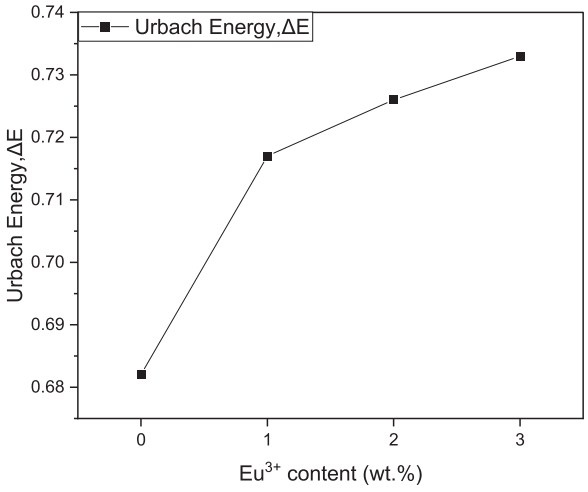

Figure 6. Urbach energy of the ZnO–B_2O_3–GB incorporated with different Eu^{3+} content.

3.6. Urbach energy analysis

Urbach energy is the optical parameter that describes the defect states in the optical band gap region. The creation of an absorption tail in the absorption spectrum is due to these localized states of a defect in the band gap region. Hence, it is referred to as the Urbach tail, and its energy is known as Urbach energy [39]. The relationship between the exponential absorption tails and the Urbach energy is as follows [40]:

$$\alpha(v) = Bexp\frac{hv}{\Delta E} \tag{5}$$

where $\alpha(v)$ = absorption coefficient, B is the constant, hv = photon energy, and ΔE = Urbach energy. The Urbach energy is determined by taking the reciprocal of the slope of the curves drawn between $\ln(\alpha)$ and hv. The plotted graph for Urbach energy of ZnO–B_2O_3–GB glass with different Eu^{3+} content is depicted in Figure 6, and the value is illustrated in Table 3.

The Urbach energies of the samples are located within a range from 0.682 to 0.733, as listed in Table 3, appropriate for amorphous materials [41], as agreed by XRD results. The Urbach energy exhibits an increment trend with an increase in Eu^{3+} content, indicating the formation of defects and growth in disorder in the glass samples. A higher Urbach energy equates to less structural stability, which means more amorphous. The rise in the Urbach energy is due to the increase in Eu^{3+} dopant, where Eu^{3+} serves as the glass modifier when incorporated into the $ZnO–B_2O_3–GB$ glass system. It presents the possibility of elongated range order locally arising from the bonding defects, which induce localized states in the glasses, resulting in the drop in optical band gap as shown from the prior result and an increased defect concentration and width of the energy tail [42]. Recently published research reported a similar tendency when Eu^{3+} ion was doped with potassium titano telluroborate glasses [13].

3.7. Optical transmittance analysis

Glass transmittance is a significant characteristic in the design and development of innovative optical components. The equation (6) was used to determine the percentage of transmittance [43], and the transmittance spectra of the glass sample are shown in Figure 7.

$$T(\%) = 100 \times 10^{-A} \tag{6}$$

where A is the absorbance.

The transmittance of all the samples over the 400–1000 nm range is approximately 70%–75%. For sample coded ZBS, 1Eu, and 2Eu, the transmittance initially steeply climbs to 70% in the visible region (400 nm–600 nm), then slightly increases to 75% in the visible and near-infrared region (600 nm–1000 nm). The sample with 3 wt.% Eu^{3+} indicates the highest transmittance among the other sample in the visible region (400 nm – 600 nm). Therefore, it reveals the $ZnO–B_2O_3–GB$ glass with and without incorporation with different Eu^{3+} ions have good transmittance in the visible region.

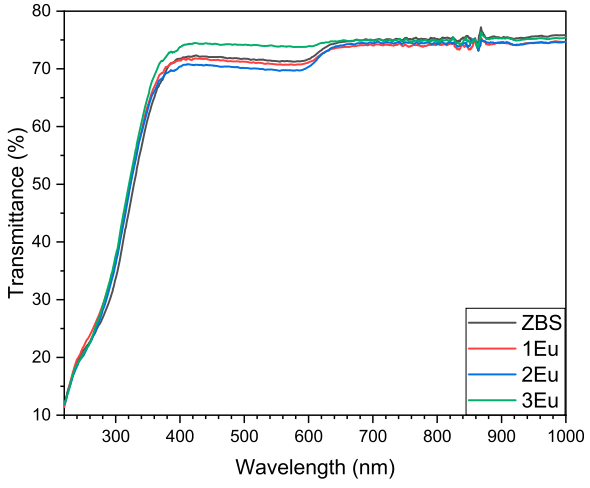

Figure 7. Transmittance spectra of $ZnO–B_2O_3–GB$ incorporated with different Eu^{3+} content.

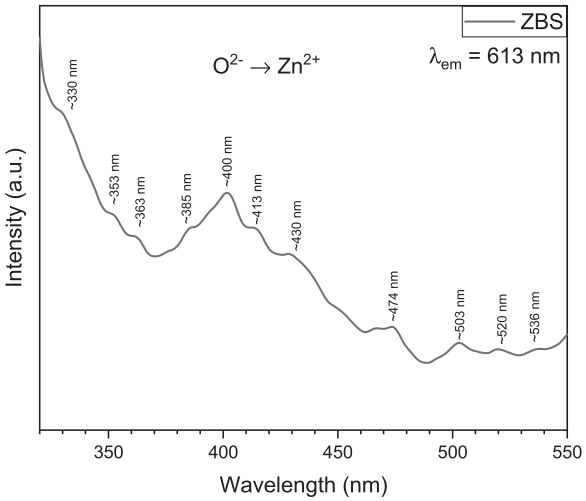

Figure 8. PLE spectra of the $ZnO–B_2O_3–GB$ glass sample.

3.8. Photoluminescence excitation spectral analysis

The photoluminescence excitation (PLE) of the host, $ZnO–B_2O_3–GB$ glass sample is shown in Figure 8. According to Figure 8, eleven peaks appear at 330, 353, 363, 385, 400, 413, 430, 474, 503, 520, and 536 nm, with the fixed wavelength emission at 613 nm, for the $ZnO–B_2O_3–GB$ glass sample. Among these peaks, the peak at wavelength 400 nm indicates the most intense peak. These peaks indicate the electron transfer of the ZnO from the valance band (VB) to the conduction band (CB), where the VB and CB are made up of *2p* oxygen orbitals and *3d* orbitals of Zn, respectively [44,45]. In other words, the excitation of the host is associated in the ZnO with the charge transfer transitions of $O^{2-} \rightarrow Zn^{2+}$ [46]. The PLE spectra of the $ZnO–B_2O_3–GB$ incorporated with different Eu^{3+} content with the emission monitor at 612 nm is despite in Figure 9. When the Eu^{3+} dopant is incorporated into the host, $ZnO–B_2O_3–GB$ glass system, the transition of the Eu^{3+} ions become dominant in the glass system. It can be observed that the PLE spectrum has multiple peak bandwidths ranging from 330 nm to 550 nm. The presence of excitation peaks correspond to the transition $^7F_0 \rightarrow {}^5H_6$ (330 nm), $^7F_0 \rightarrow {}^5D_4$ (352 nm), $^7F_0 \rightarrow {}^5L_7$ (385 nm), $^7F_0 \rightarrow {}^5L_6$ (400 nm), $^7F_0 \rightarrow {}^5D_3$ (414 nm), $^7F_0 \rightarrow {}^5D_2$ (473 nm), $^7F_0 \rightarrow {}^5D_1$ (502, 520, 536 nm) [47,48]. The excitation spectra include the near ultraviolet and blue light regions; therefore, the materials could be effectively excited by the near-ultraviolet and blue LED chips [49]. Among the peaks, the major excitation peak is located at 400 nm, similar to the host. Hence, 400 nm is chosen as the excitation wavelength to study the PL emission of the glass sample to emit intense reddish-orange emission.

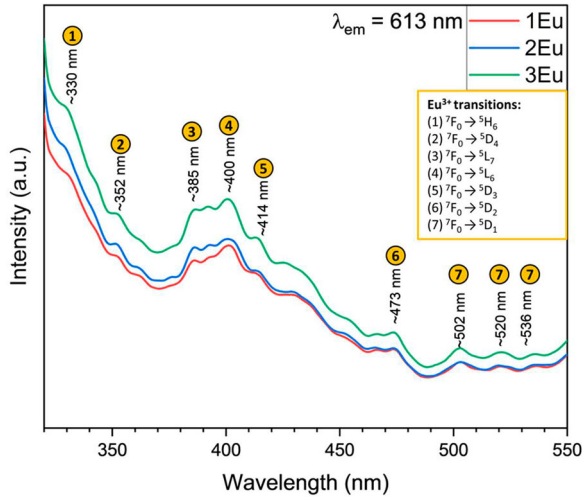

Figure 9. PLE spectra of the ZnO–B_2O_3–GB incorporated with different Eu^{3+} content.

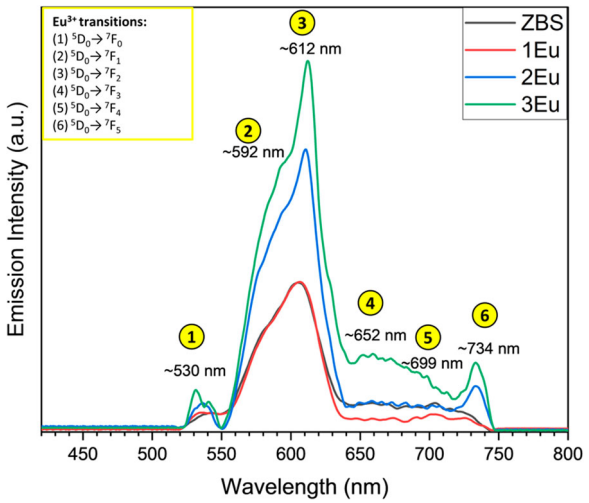

Figure 10. PL emission spectra glass samples excited at wavelength 400 nm.

3.9. Photoluminescence emission spectral analysis

Figure 10 indicates the glass samples' photoluminescence (PL) emission spectrum excited at 400 nm. From Figure 10, the glass sample coded ZBS, without Eu^{3+} incorporated into the ZnO–B_2O_3–GB glass system, indicates three emission peaks at 530 nm (green), 574 nm (yellow), and 707 (red). The green emission of the ZnO–B_2O_3–GB glass could be due to the zinc vacancies inside the ZnO [50]. Generally, the defect states that occur in ZnO are zinc vacancies (V_{Zn}), oxygen vacancies (V_O), zinc interstitial (Zn_i), oxygen interstitial (O_i), and oxygen antisite (O_{Zn}) [46]. Since zinc vacancies are the deep acceptors, they are more likely to be where the green luminescence in ZnO originates [51]. Furthermore, the SiO_2 matrix could have also reflected the UV emission. There are two possible mechanisms by which the surface interaction between ZnO particles and the SiO_2 matrix could increase the UV-emission of the ZnO–B_2O_3–GB glass sample. First, the SiO_2 matrix altered the surface properties of ZnO particles, leading to a decrease in the density of surface dangling bonds and concentrations of O^{2-} ions in the Zn-O-Si. It decreased the likelihood of non-radiative ions and visible emission, which enhanced UV emission. Second, the surface interaction between ZnO and SiO_2 could influence the UV-photoluminescence enhancement by developing interface states where the carrier can be trapped and recombined to emit UV light [52]. Meanwhile, the green region (530 nm) appears in the ZnO–B_2O_3–GB glass related to the transition from the conduction band to oxygen vacancies (CB → V_O) [53]. The zinc interstitial transition ($Zn_i^+ \rightarrow V_{Zn}^-$) gives the yellow emission at 574 nm [54]. On the other hand, the emission of 707 nm (red) is due to the transition from the conduction band to oxygen interstitials (CB → O_i) [53]. The ZnO–B_2O_3–GB glass's green, yellow, and red emissions were thereby affected by a defect in

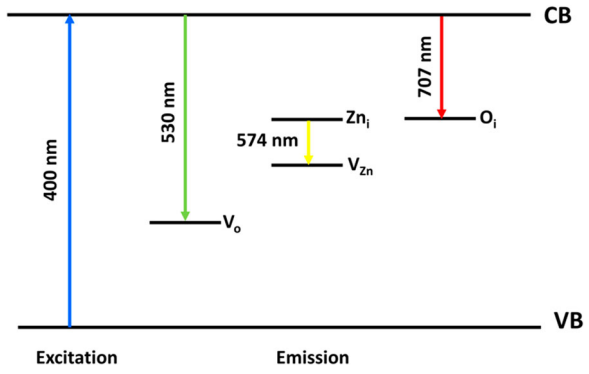

Figure 11. Schematic band structures diagram of ZnO in the ZnO–B_2O_3–GB glass system.

the ZnO particle and aided by SiO_2. In the meantime, the schematic band structures diagram of ZnO in the ZnO–B_2O_3–GB glass system is shown in Figure 11.

In contrast, when the glass samples are incorporated with Eu^{3+} ions, several new emission spectra start to appear due to the presence of Eu^{3+} ions. Moreover, the PL emission band trend shifts to a higher wavelength as the Eu^{3+} dopant increases. Therefore, when the Eu^{3+} dopant increases up to 3 wt.%, the emission band emerges at 578 nm (yellow), 592 nm (orange), 612 nm (reddish-orange), 652 nm (red), 699 nm (red), and 734 nm (red). Meanwhile, once excited at 400 nm, the Eu^{3+} ions will originally be excited from $^7F_0$ to the $^5L_6$ state. Then, the Eu^{3+} ions relax to the $^5D_2$ state by populating it and subsequently populating the low-lying $^5D_1$ and $^5D_0$ energy levels non-radiatively, with emission of transitions from metastable state $^5D_0$ to ^7F_J, where $\Delta J = 0$ to 5 [47,55]. The energy transition $^5D_0 \rightarrow {}^7F_J$ ($J = 0, 1, 2, 3, 4, 5$) designated to 578, 592, 612, 652, 699, and 734 nm, respectively. The energy level diagram for the transitions of Eu^{3+} in the ZnO–B_2O_3–GB glass system is depicted in Figure 12.

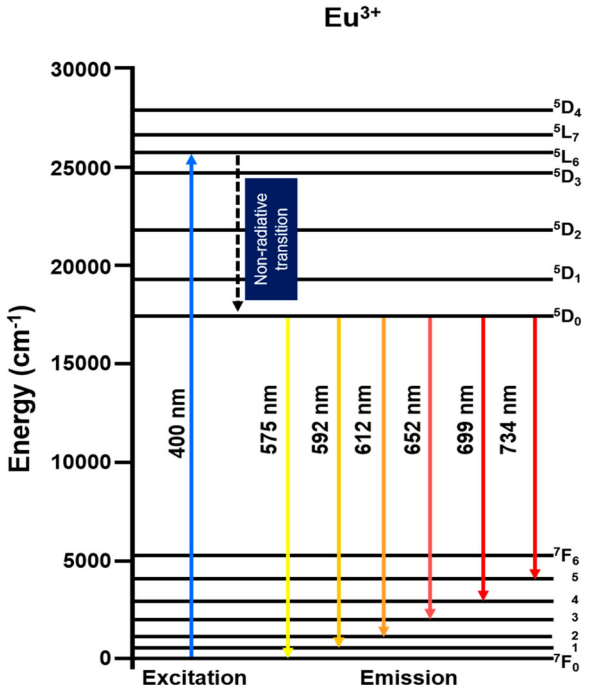

Figure 12. Energy level diagram of Eu^{3+} in $ZnO–B_2O_3–GB$ glass system.

The dipole emission transition $^5D_0 \rightarrow {}^7F_0$ (578 nm) is environmentally sensitive and is forbidden according to parity selection rules, where $\Delta J = 0$ and the transition from $\Delta J = 0 \rightarrow 0$ indicate forbidden. Additionally, the ground state $^7F_0$ and the first excited state $^5D_0$ are non-degenerate, regardless of the symmetry [55]. In the meantime, the transition $^5D_0 \rightarrow {}^7F_1$ (592 nm) belongs to the magnetic dipole (MD) transitions which obey the selection rule shown in Table 4, where $\Delta J = \pm 1$. It is independent of the host matrix, which suggests that its intensity is unaltered by the local symmetry [56]. The $^5D_0 \rightarrow {}^7F_2$ (612 nm) is attributed to magnetic dipole (MD) transitions, which follow the selection rule [57] shown in Table 4, where $\Delta J = \pm 2$. It is hypersensitive and highly influenced by the symmetry of the Eu^{3+} ions' local environment. The electric dipole transition is only possible if the Eu^{3+} ion is in a location without an inversion centre [58]. The $^5D_0 \rightarrow {}^7F_3$ (652 nm) have transitions with a mixed character (MD and ED) owing to J-mixing, aided by the host matrix's significant crystal-field effects. It reveals that the Eu^{3+} ions are asymmetrically located in the matrix. Furthermore, the $^5D_0 \rightarrow {}^7F_4$ (699 nm) induced electric dipole transition due to $\Delta J = \pm 4$, and $^5D_0 \rightarrow {}^7F_5$ (734 nm) belong forbidden owing to the J-mixing effect between multiplets. The analysis of emission transitions performed by the published findings [37,38,40] and the summarized emission transition are listed in Table 5. Based on Figure 11, the reddish-orange emission at 612 nm ($^5D_0 \rightarrow {}^7F_2$) indicates the most intense emission among all the emissions. Moreover, the $^5D_0 \rightarrow {}^7F_2$ transition is more robust than the $^5D_0 \rightarrow {}^7F_1$, implying that Eu^{3+} is found in low symmetry sites. Therefore, the intense emission at 612 nm suggests that the Eu^{3+} incorporated $ZnO–B_2O_3–GB$ glass potential to be reddish-orange emitting materials [59]. Indeed, the intensity of the emission increase as progression on the Eu^{3+} dopant, and the sample with 3 wt.% Eu^{3+} dopants indicate the highest emission intensity among the other content of Eu^{3+} dopants in this work. Thus, it can be said that the optimum dopant of Eu^{3+} incorporated into the $ZnO–B_2O_3–GB$ glass system is 3 wt.% among the other Eu^{3+} dopants content (0, 1, and 2 wt.%) in current work.

3.10. CIE 1931 chromaticity analysis

The Commission International d'Eclairage (CIE) 1931 is used to analyze the dominant emission colour of Eu^{3+} incorporated into the $ZnO–B_2O_3–GB$ glass system. The CIE 1931 diagram is a widely acknowledged technique for representing any colour's component using the primary colours: red, blue, and green [56]. The CIE 1931 chromaticity is shown in Figure 13. The chromaticity coordinates, dominant wavelength, CCT, and colour purity of the glass samples are listed in Table 6. Based on Figure 13, the CIE coordinate of ZBS found at (0.4692, 0.5071), which falls in the yellow-orange region, while its dominant wavelength is 575.1 nm. On

Table 4. Selection rules for electric dipole transitions and magnetic dipole transitions.

Transitions	Selection rules	References
Electric dipole (ED) transitions	$\Delta S = 0$; $\Delta l = \pm 1$; ΔL, $\Delta J \leq 6$ unless J or J′ = 0 when $\Delta J = 2, 4, 6$	[57]
Magnetic dipole (MD) transitions	$\Delta S = \Delta L = 0$; $\Delta J \leq 1$, except 0→0; $\Delta l = 0$	

Table 5. Emission transition and its colour for the designated emission wavelength.

Emission wavelength (nm)	Colour	Emission transition	Transition assignment
578	Yellow	$^5D_0 \rightarrow {}^7F_0$	Forbidden
592	Orange	$^5D_0 \rightarrow {}^7F_1$	MD
612	Reddish-orange	$^5D_0 \rightarrow {}^7F_2$	ED
652	Red	$^5D_0 \rightarrow {}^7F_3$	Forbidden
699	Deep red	$^5D_0 \rightarrow {}^7F_4$	ED
734	Deep red	$^5D_0 \rightarrow {}^7F_5$	Forbidden

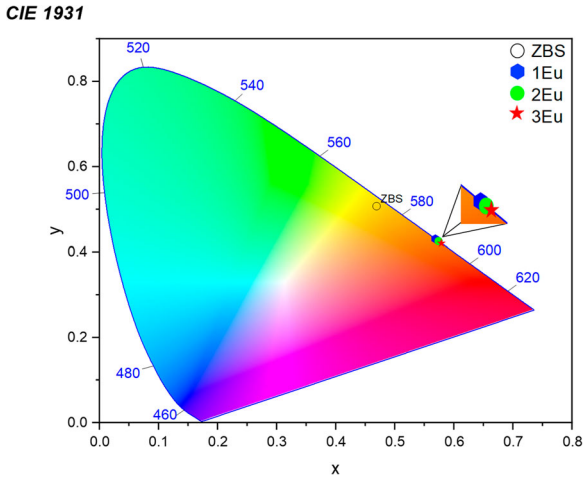

Figure 13. CIE 1931 chromaticity of the ZnO–B_2O_3–GB incorporated with different Eu^{3+} content.

the other hand, when the Eu^{3+} is incorporated into the ZnO–B_2O_3–GB glass system, the chromaticity coordinates are located in the reddish-orange region. The CIE coordinates (0.5687, 0.4304), (0.5741, 0.4251), and (0.5790, 0.4201) belong to 1Eu, 2Eu, and 3Eu glass samples, respectively.

Meanwhile, the dominant wavelength increased from 575.1 nm to 590.7 nm, indicating that the samples shifted from yellow to reddish-orange. Figure 14 shows the ZnO–B_2O_3–GB glass sample under UV lamp excites at 365 nm wavelength. The calculated CIE coordinates for Eu^{3+} incorporated ZnO–B_2O_3–GB glass are near the Amber LED NSPAR 70BS produced by Nichia Corporation (0.570, 0.420) [60]. Moreover, Cao and the coworker also reported a similar CIE coordinate at (0.5732, 4262) in $Ca_3La_6Si_6O_{24}$:Eu^{3+} phosphor [48]. The correlated colour temperature (CCT) is typically required to evaluate the quality of light emitted by the glasses. The calculated CCT value dropped from 3220 K (ZBS) to 1673 K (3Eu) when the Eu^{3+} incorporated ZnO–B_2O_3–GB glass. The CCT value, ~1600 K, is less than the fluorescent tube (3935 K) [33], and it indicates the samples with Eu^{3+} dopant have bright reddish-orange emission. Moreover, the samples' colour purity reveals a high value, at 99%, implying that they meet the basic criteria for field emission displays. Thus, the excellent colour purity of the Eu^{3+} incorporated ZnO–B_2O_3–GB glass suggests it is ideal for reddish-orange LED applications.

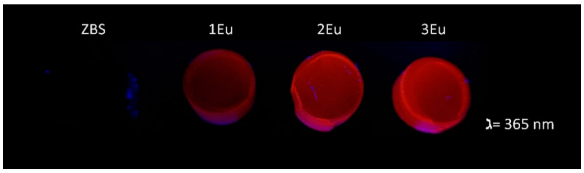

Figure 14. The ZnO–B_2O_3–GB glass sample under UV lamp excites at 365 nm wavelength.

4. Conclusion

To sum up, the zinc-borosilicate glass incorporated with Eu^{3+} derived from the waste glass bottle was successfully synthesized via the conventical melt-quenching method. XRD and FTIR proved amorphous in the glass sample. The absorption spectra imply the transition of Eu^{3+} present in the UV-visible region at ~394 nm attributed to the 4f–4f transition. The optical band gap for direct and indirect band gap reveals a decreasing trend as the Eu^{3+} dopant increases. The increase in Eu^{3+} dopant led to the rise in NBOs, resulting in the glass structure becoming more disordered. Additionally, the refractive index and Urbach energy trend increase with increasing the Eu^{3+} content. Besides, the emission at 612 nm ($^5D_0 \rightarrow {}^7F_2$) in the PL spectrum indicates the most intense emission among all the emissions when excited at 400 nm. This work's optimal content for Eu^{3+} incorporated ZnO–B_2O_3–GB glass is 3 wt.% among the other Eu^{3+} dopants content (0, 1, and 2 wt.%), which gives the highest emission intensity. In the meantime, the CIE chromaticity coordinates reveal the samples incorporated with Eu^{3+} located in the reddish-orange region. Therefore, the findings suggest that the ZnO–B_2O_3–GB glass potential be utilized in optoelectronic applications such as reddish-orange LED lighting.

CRediT authorship contribution statement

Wei Mun Cheong: Conceptualization, Methodology, Software, Formal analysis, Investigation, Data Curation, Writing – Original Draft, Visualization. **Mohd Hafiz Mohd Zaid**: Conceptualization, Methodology, Formal analysis, Data Curation, Writing – Original Draft, Supervision, Project administration, Funding acquisition. **Khamirul Amin Matori**, **Yap Wing Fen**, **Tan Sin Tee**: Formal analysis, Data Curation, Writing – Review & Editing, Supervision. **Zhi Wei Loh**: Conceptualization, Methodology, Software, Formal analysis, Investigation,

Table 6. Chromaticity coordinates, dominant wavelength, CCT, and colour purity of the glass samples.

Glass Sample	Chromaticity coordinates (x,y)	Dominant wavelength (nm)	CCT (K)	Colour purity (%)
ZBS	0.4692, 0.5071	575.1	3220	93.2
1Eu	0.5687, 0.4304	589.0	1791	99.9
2Eu	0.5741, 0.4251	589.8	1729	99.9
3Eu	0.5790, 0.4201	590.7	1673	99.9

Data Curation, Writing – Review & Editing. **Mohd Zul Hilmi Mayzan**: Methodology, Software, Formal analysis, Data Curation.

Declaration of competing interest

The authors declared that they have no conflicts of interest to this work.

Acknowledgments

This research was supported by the Universiti Putra Malaysia through the Geran Putra Berimpak (GP-GPB/2021/9702600) for this research work.

Disclosure statement

No potential conflict of interest was reported by the author(s).

Funding

This work was supported by Universiti Putra Malaysia [grant number: Geran Putra Berimpak (GP-GPB/2021/9702600)].

ORCID

Mohd Hafiz Mohd Zaid http://orcid.org/0000-0001-6734-800X

References

[1] Xiang J, Yang J, Luo N, et al. Optimized photoluminescence and electronic properties of europium doped phosphate red phosphor. Results Phys. 2019;13:102258. doi:10.1016/j.rinp.2019.102258

[2] Mao W, Cai M, Xie W, et al. Tunable white light in trivalent europium single doped tin fluorophosphates ultra-low melting glass. J Alloys Compd. 2019;805:205–210. doi:10.1016/j.jallcom.2019.07.014

[3] Omri K, Lahouli R. Tunable dielectric and microstructure properties Zn_2SiO_4-Mn glass-ceramics for multifunctional applications. J Mater Sci Mater Electron. 2019;30:7834–7839. doi:10.1007/s10854-019-01102-9

[4] Xiao Y, Wu Z, Yao Q, et al. Luminescent metal nanoclusters: Biosensing strategies and bioimaging applications. Aggregate. 2021;2:114–132. doi:10.1002/agt2.11

[5] Li K, Zhu D, Lian H. Up-conversion luminescence and optical temperature sensing properties in novel KBaY$(MoO_4)_3$:Yb^{3+},Er^{3+} materials for temperature sensors. J Alloys Compd. 2020;816:152554. doi:10.1016/j.jallcom.2019.152554

[6] Li K, Zhu D, Yue C. Exceptional low-temperature fluorescence sensing properties in novel KBaY(MoO4)3:Yb^{3+}, Ho^{3+} materials based on FIR of Ho^{3+} transitions $^5F_{5(1)} \rightarrow {}^5I_8/{}^5S_2 \rightarrow {}^5I_8$. J Mater Chem C. 2022;10:6603–6610. doi:10.1039/D2TC01061E

[7] Kesarwani V, Rai VK. Optical thermometry and broad infrared luminescence in highly sensitized TBO glass. Opt Laser Technol. 2022;146:107535. doi:10.1016/j.optlastec.2021.107535

[8] Zagrai M, Suciu RC, Rada S, et al. Structural and optical properties of Eu^{3+} ions in lead glass for photonic applications. J Non Cryst Solids. 2021;569:120988. doi:10.1016/j.jnoncrysol.2021.120988

[9] Jaafar SH, Zaid MHM, Matori KA, et al. Effect of sintering temperatures and foaming agent content to the physical and structural properties of wollastonite based foam glass-ceramics. Sci Sinter. 2020;52:269–281. doi:10.2298/SOS2003269J

[10] Cheong WM, Zaid MHM, Matori KA, et al. Structural, elastic and mechanical analysis of samarium doped zinc-borosilicate glass. Optik (Stuttg). 2022;267:169658. doi:10.1016/j.ijleo.2022.169658

[11] Zaid MHM, Matori KA, Wah LC, et al. Elastic moduli prediction and correlation in soda lime silicate glasses containing ZnO. Int J Phys Sci. 2011;6:1404–1410. doi:10.5897/IJPS11.111

[12] Vander Stouw GJ, Sundaram SK. Thermal stability of crystalline phases in MnO-doped zinc borosilicate glasses. Appl Phys A Mater Sci Process. 2020;126:1–13. doi:10.1007/s00339-020-03750-9

[13] Mariselvam K, Liu J. Synthesis and luminescence properties of Eu3+ doped potassium titano telluroborate (KTTB) glasses for red laser applications. J Lumin. 2021;230:117735. doi:10.1016/j.jlumin.2020.117735

[14] Elkholy H, Othman H, Hager I, et al. Europium-doped tellurite glasses: the Eu^{2+} emission in tellurite, adjusting Eu^{2+} and Eu^{3+} emissions toward white light emission. Materials (Basel). 2019;12:4140. doi:10.3390/ma12244140

[15] Rajaramakrishna R, Nijapai P, Kidkhunthod P, et al. Molecular dynamics simulation and luminescence properties of Eu3+ doped molybdenum gadolinium borate glasses for red emission. J Alloys Compd. 2020;813:151914. doi:10.1016/j.jallcom.2019.151914

[16] Geng X, Xie Y, Ma Y, et al. Abnormal thermal quenching and application for w-LEDs: Double perovskite Ca2InSbO6:Eu3+ red-emitting phosphor. J Alloys Compd. 2020;847:156249. doi:10.1016/j.jallcom.2020.156249

[17] Effendy N, Zaid MHM, Sidek HAA, et al. Influence of ZnO to the physical, elastic and gamma radiation shielding properties of the tellurite glass system using MCNP-5 simulation code. Radiat Phys Chem. 2021;188:109665. doi:10.1016/j.radphyschem.2021.109665

[18] Babu BC, Rao BV, Ravi M, et al. Structural, microstructural, optical, and dielectric properties of Mn2+: Willemite Zn_2SiO_4 nanocomposites obtained by a sol-gel method. J Mol Struct. 2017;1127:6–14. doi:10.1016/j.molstruc.2016.07.074

[19] Wahab SAA, Matori KA, Aziz SHA, et al. Synthesis of cobalt oxide Co_3O_4 doped zinc silicate based glass-ceramic derived for LED applications. Optik (Stuttg). 2019;179:919–926. doi:10.1016/j.ijleo.2018.11.025

[20] Markovska I, Dimitrov T. Synthesis and characterization of willemite ceramic pigments suitable for the ceramic industry by utilization of rice husk ash. J Chem Biol Phys Sci. 2019;9; doi:10.24214/jcbps.a.9.4.21932

[21] Ibreva T, Dimitrov T, Titorenkova R, et al. Synthesis and characterization of willemite ceramic pigments in the system xCoO. (2–x)ZnO. SiO_2. Bulg Chem Commun. 2018;50:31–37.

[22] Ceniceros-Orozco VE, Escorcia-García J, Gutiérrez-Chavarría CA, et al. Orange-reddish photoluminescence enhancement and wollastonite nanocrystals formation induced by CaO in Sm3+-doped calcium sodium borosilicate glasses. Ceram Int. 2022. doi:10.1016/j.ceramint.2022.01.347

[23] Halimah MK, Asyikin AS, Nazrin SN, et al. Influence of erbium oxide on structural, physical, elastic and luminescence properties of rice husk biosilicate zinc borotellurite glasses for laser application. J Non Cryst Solids. 2020: 1–7. doi:10.1016/j.jnoncrysol.2020.120467

[24] Khaidir REM, Fen YW, Zaid MHM, et al. Exploring Eu^{3+}-doped ZnO-SiO_2 glass derived by recycling renewable source of waste rice husk for white-LEDs application. Results Phys. 2019;15. doi:10.1016/j.rinp.2019.102596
[25] Kawano N, Shinozaki K, Kato T, et al. Radiation response properties of Eu^{3+}-doped K_2O–Ta_2O_5–Ga_2O_3 glasses. Ceram. Int. 2022;48:9353–9361. doi:10.1016/j.ceramint.2021.12.130
[26] Monisha M, Murari MS, Sayyed MI, et al. Thermal, structural and optical behaviour of Eu^{3+} ions in Zinc Alumino Boro-Silicate glasses for bright red emissions. Mater Chem Phys. 2021;270:124787. doi:10.1016/j.matchemphys.2021.124787
[27] Jaafar SH, Mohd Zaid MH, Matori KA, et al. Synthesis of Eu3+-doped ZnO/Zn2SiO4 composite phosphor for potent optoelectronic applications. Brazilian J Phys. 2022;52. doi:10.1007/s13538-021-01017-z
[28] Hajer SS, Halimah MK, Azmi Z, et al. Effect of samarium nanoparticles on optical properties of zinc borotellurite glass system. Mater Sci Forum. 2016;846:63–68. doi:10.4028/www.scientific.net/MSF.846.63
[29] Makuła P, Pacia M, Macyk W. How to correctly determine the band gap energy of modified semiconductor photocatalysts based on UV-Vis Spectra. J Phys Chem Lett. 2018;9:6814–6817. doi:10.1021/acs.jpclett.8b02892
[30] Singh R, Bedyal AK, Manhas M, et al. Charge compensated CaSr2(PO4)2:Sm3+, Li+/Na+/K+ phosphor: Luminescence and thermometric studies. J Alloys Compd. 2022;901:163793. doi:10.1016/j.jallcom.2022.163793
[31] Al-Hadeethi Y, Ahmed M, Al-Heniti SH, et al. Rare earth Co-Doped tellurite glass ceramics: Potential use in optical and radiation shielding applications. Ceram Int. 2020;46:19198–19208. doi:10.1016/j.ceramint.2020.04.257
[32] Fadhilah Zalamin SN, Mohd Zaid MH, Matori KA, et al. Comprehensive study on optical and luminescence properties of Sm^{3+} doped magnesium borotellurite glasses. J Phys Chem Solids. 2022;163:110563. doi:10.1016/j.jpcs.2021.110563
[33] Ullah I, Khan I, Shah SK, et al. Luminescence properties of Sm3+ doped Na2B4O7 glasses for lighting application. J Lumin. 2021;230:117700. doi:10.1016/j.jlumin.2020.117700
[34] Al-Harbi N, Sayyed MI, Al-Hadeethi Y, et al. A novel CaO–K_2O–Na_2O–P_2O_5 glass systems for radiation shielding applications. Radiat. Phys. Chem. 2021;188; doi:10.1016/j.radphyschem.2021.109645
[35] Wahab EAA, Shaaban KS, Al-Baradi AM. Enhancement of optical and physical parameters of lead zinc silicate glasses by doping W^{+3} ions. Silicon. 2021. doi:10.1007/s12633-021-01236-8
[36] Abu-Khadra AS, Taha AM, Abdel-Ghany AM, et al. Effect of silver iodide (AgI) on structural and optical properties of cobalt doped lead-borate glasses. Ceram Int. 2021;47:26271–26279. doi:10.1016/j.ceramint.2021.06.036
[37] Shaari HR, Azlan MN, Azlina Y, et al. Investigation of Structural and optical properties of graphene oxide-coated neodymium nanoparticles doped zinc-tellurite glass for glass fiber. J Inorg Organomet Polym Mater. 2021;31:4349–4359. doi:10.1007/s10904-021-02061-7
[38] Abouhaswa AS, Sayyed MI, Altowyan AS, et al. Evaluation of optical and gamma ray shielding features for tungsten-based bismuth borate glasses. Opt Mater (Amst). 2020;106:109981. doi:10.1016/j.optmat.2020.109981
[39] Paswan SK, Kumari S, Kar M, et al. Optimization of structure-property relationships in nickel ferrite nano particles annealed at different temperature. J Phys Chem Solids. 2021;151:109928. doi:10.1016/j.jpcs.2020.109928
[40] Essalah G, Kadim G, Jabar A, et al. Structural, optical, photoluminescence properties and Ab initio calculations of new Zn2SiO4/ZnO composite for white light emitting diodes. Ceram Int. 2020;46:12656–12664. doi:10.1016/j.ceramint.2020.02.031
[41] Stalin S, Gaikwad DK, Al-Buriahi MS, et al. Influence of Bi2O3/WO3 substitution on the optical, mechanical, chemical durability and gamma ray shielding properties of lithium-borate glasses. Ceram Int. 2020. doi:10.1016/j.ceramint.2020.10.109
[42] Zhang X, Zhang J, Zhou C, et al. High refractive index of Eu^{3+} doped La_2O_3-TiO_2-Nb_2O_5-WO_3 oxide glasses with low wavelength dispersion. J Non Cryst Solids. 2022;581:121228. doi:10.1016/j.jnoncrysol.2021.121228
[43] Ezenwaka LN, Umeokwonna NS, Okoli NL. Optical, structural, morphological, and compositional properties of cobalt doped tin oxide (CTO) thin films deposited by modified chemical bath method in alkaline medium. Ceram Int. 2020;46:6318–6325. doi:10.1016/j.ceramint.2019.11.106
[44] Galdámez-Martinez A, Santana G, Güell F, et al. Photoluminescence of ZnO nanowires: a review. Nanomaterials. 2020;10:857. doi:10.3390/nano10050857
[45] Lima SAM, Sigoli FA, Jafelicci JM, et al. Luminescent properties and lattice defects correlation on zinc oxide. Int J Inorg Mater. 2001;3:749–754. doi:10.1016/S1466-6049(01)00055-1
[46] Mazabuel-Collazos A, Gómez CD, Rodríguez-Páez EJ. ZnO-TiO2 nanocomposites synthesized by wet-chemical route: Study of their structural and optical properties. Mater Chem Phys. 2019;222:230–245. doi:10.1016/j.matchemphys.2018.10.007
[47] Cao R, Liang H, Chen T, et al. Study on luminescence characterizations of $SrMg_2La_2W_2O_{12}$:Eu^{3+} red-emitting phosphor. J Phys Chem Solids. 2022;163:110569. doi:10.1016/j.jpcs.2021.110569
[48] Cao R, Lv X, Jiao Y, et al. $Ca_3La_6Si_6O_{24}$:Eu^{3+} orange-red-emitting phosphor: synthesis, structure and luminescence properties. Mater Res Bull. 2020;122:110651. doi:10.1016/j.materresbull.2019.110651
[49] Shi Y, Xu Y, Hu W, et al. Energy transfer effect in novel Sm^{3+}-Eu^{3+} co-activated $CaMgAl_{10}O_{17}$ phosphors. Optik (Stuttg). 2020;202:163599. doi:10.1016/j.ijleo.2019.163599
[50] Wahab SAA, Matori KA, Aziz SHA, et al. Effect of ZnO on the phase transformation and optical properties of silicate glass frits using rice husk ash as a SiO_2 source. J Mater Res Technol. 2020;9:11013–11021. doi:10.1016/j.jmrt.2020.08.005
[51] Janotti A, Van De Walle CG. Fundamentals of zinc oxide as a semiconductor. Reports Prog Phys. 2009;72; doi:10.1088/0034-4885/72/12/126501
[52] Fu Z, Yang B, Li L, et al. An intense ultraviolet photoluminescence in sol-gel ZnO-SiO_2 nanocomposites. J Phys Condens Matter. 2003;15:2867–2873. doi:10.1088/0953-8984/15/17/335
[53] Dey S, Das S, Kar AK. Role of precursor dependent nanostructures of ZnO on its optical and photocatalytic activity and influence of FRET between ZnO and methylene blue dye on photocatalysis. Mater Chem Phys.

2021;270:124872. doi:10.1016/j.matchemphys.2021.124872

[54] Ferreira NS, Sasaki JM, Silva RS, et al. Visible-light-responsive photocatalytic activity significantly enhanced by active [V_{Zn}^{+} V_{O}^{+}] defects in self-assembled ZnO nanoparticles. Inorg Chem. 2021;60:4475–4496. doi:10.1021/acs.inorgchem.0c03327

[55] Naresh V, Rudramadevi BH, Buddhudu S. Crossrelaxations and non-radiative energy transfer from (4G5/2) Sm3+→ (5D0) Eu3+: B2O3–ZnO glasses. J Alloys Compd. 2015;632:59–67. doi:10.1016/j.jallcom.2015.01.138

[56] Nagaraj R, Raja A, Ranjith S. Synthesis and luminescence properties of novel red-emitting Eu3+ ions doped silicate phosphors for photonic applications. J Alloys Compd. 2020;827:154289. doi:10.1016/j.jallcom.2020.154289

[57] Kam CH, Buddhudu S. Photoluminescence properties of Eu3+:ZrF4–BaF2–LaF3–YF3–AlF3–NaF glasses. Phys. B Condens. Matter. 2004;344:182–189. doi:10.1016/j.physb.2003.09.256

[58] Selvi S, Marimuthu K, Suriya Murthy N, et al. Red light generation through the lead boro−telluro−phosphate glasses activated by Eu3+ ions. J. Mol. Struct. 2016;1119:276–285. doi:10.1016/j.molstruc.2016.04.073

[59] Meng X, Huang S, Shang M. Red emitting Ba2GdVO6:Eu3+ phosphors for blue light converted warm white LEDs. Inorg Chem Commun. 2020;113:107768. doi:10.1016/j.inoche.2020.107768

[60] Singh V, Kaur S, Jayasimhadri M. Luminescence properties of orange emitting $CaAl_4O_7:Sm^{3+}$ phosphor for solid state lighting applications. Solid State Sci. 2020;101:106049. doi:10.1016/j.solidstatesciences.2019.106049